When $\delta\alpha$ becomes larger than the QPC opening angle Φ for higher V_i, one can clearly observe the expected dip in forward direction ($V_i > 3.0$ mV, Fig. 4a). The amplitude of the dip is much larger than would be the case for a 3D electron system.

As discussed above, the local approximation of Eqn (5) is not valid at small scattering angles $\alpha < \Phi$. For these angles, $g(\alpha)$ is more precisely given by the integral equation:

$$\delta V_d^s \simeq 2Cv \int d\varphi \rho_i(\varphi) \int d\varphi' \rho_d(\varphi') \times \tilde{g}\left(\varphi' - \varphi + \frac{L}{r_c}, V_i\right) \kappa\left(\varphi' - \varphi + \frac{L}{r_c}\right), \quad (9)$$

where $\kappa(x) = 1/|x|$ for $x > \Phi$ and $\kappa(x) = 1/\Phi$ for $x < \Phi$. Here again we use $\tilde{g}(\alpha)$ as defined in Eqn (6);

$$\Lambda = L \frac{2\varphi' + L/r_c}{2(\varphi' - \varphi + L/r_c)}$$

is the distance between injector and the crossing point (O) of electron trajectories injected at angle φ and detected at angle φ'; the integration in Eqn (9) has to be evaluated for all Λ such that $0 < \Lambda < L$, while $l_{ee} \equiv l_{ee}(V_i)$.

In conclusion, electron-beam experiments in the 2DEG of GaAs/(Ga,Al)As heterostructures demonstrate unambiguously the occurrence of small-angle ee-scattering characterizing the dimensionality effect on the momentum relaxation in 2D systems. The characteristic scattering distribution function is obtained directly from magnetic-field-dependent beam deflection experiments. The scattering distribution function broadens with increasing electron energy, $\delta\alpha \propto \sqrt{eV_i/\varepsilon_F}$, in contrast to 3D systems where the width is energy-independent. Furthermore, a pronounced dip occurs at small angles. These observations represent conclusive evidence for the manifestation of 2D density-of-states effects in the ee-scattering process.

Acknowledgements. This work was supported in part by Volkswagen Stiftung (Grant I/72531) and by the DFG (MO 771/1–2).

References

1. Chaplik A V *Zh. Eksp. Teor. Fiz.* **60** 1845 (1971) [*Sov. Phys. JETP* **33** 997 (1971)]; Hodges C, Smith H, Wilkins J *Phys. Rev. B* **4** 302 (1971)
2. Guiliani G F, Quinn J J *Phys. Rev. B* **26** 4421 (1982)
3. Gurzhi R N, Kopeliovich A I, Rutkevich S B *Adv. Phys.* **36** 221 (1987); Gurzhi R N, Kalinenko A N, Kopeliovich A I *Phys. Low-Dim. Struct.* (2) 75 (1994)
4. Gurzhi R N, Kalinenko A N, Kopeliovich A I *Phys. Rev. B* **52** 4744 (1995); *Phys. Rev. Lett.* **74** 3872 (1995)
5. Gurzhi R N, Kalinenko A N, Kopeliovich A I *Fiz. Nizk. Temp.* **23** 58 (1997) [*Low Temp. Phys.* **23** 44 (1997)]
6. Laikhtman B *Phys. Rev. B* **45** 1259 (1992)
7. Buhmann H et al. *Fiz. Nizk. Temp.* **24** 978 (1998) [*Low Temp. Phys.* **24** 737 (1998)]
8. Predel H et al. *Phys. Rev. B* **62** 2057 (2000)
9. Molenkamp L W et al. *Phys. Rev. B* **41** 1274 (1990)
10. Sivan U, Heiblum M, Umbach C P *Phys. Rev. Lett.* **63** 992 (1989)
11. Callaway J *Phys. Rev.* **113** 1046 (1959)
12. Cumming D R S, Davies J H *Appl. Phys. Lett.* **69** 3363 (1996)
13. Gurzhi R N, Kalinenko A N, Kopeliovich A I *Surf. Sci.* **361/362** 497 (1996)

Submicron charge-density-wave devices

H S J van der Zant, N Marković, E Slot

Abstract. We review our fabrication methods to produce submicron charge-density-wave (CDW) structures and present measurements of CDW dynamics on a microscopic scale. Our data show that mesoscopic CDW dynamics is different from bulk behavior. We have studied current-conversion and found a size-effect that can not be accounted for by existing models. An explanation might be that the removal and addition of wave fronts becomes correlated in time when probe spacing is reduced below a few μm. On small segments we occasionally observe negative differential resistance in the $I(V)$ characteristics and sometimes the resistance may even become negative. We believe that the interplay between CDW deformations (strain) and quasi-particles may yield non-equilibrium effects that play a crucial role in this new phenomenon. No detailed theoretical calculations are available. Our measurements clearly show the need of a microscopic model for CDW dynamics.

1. Introduction

Electrical conductors with a chain-like structure may exhibit a phase transition to a collective ground state with charge-density waves (CDWs) [1]. The appearance of a CDW state is connected to the Peierls instability [2]: at low temperatures the uniform distribution of conduction electrons of a one-dimensional (1D) conductor is unstable due to their coupling to phonon modes. As a result, the lattice of atoms is distorted and the electrons condense into a ground state with a periodic modulation of the charge density. Collective transport occurs when these CDWs move along the chains. This sliding CDW motion shows similarities with transport in superconductors, with the role of current and voltage reversed. To date, CDW transport has been studied in bulk crystals and has shown many remarkable phenomena. Examples are ac current oscillations induced by a dc electric field and strongly nonlinear electrical properties.

In metallic and superconducting devices, reduction of sizes has revealed a variety of new mesoscopic phenomena. For charge-density-wave (CDW) conductors, the mesoscopic regime has not been studied in detail, largely because samples of (sub)micron sizes could not be fabricated in a controlled way. In this paper, we review our efforts to fabricate small-scale CDW devices of the CDW conductors $NbSe_3$ and o-TaS_3 (Section 2). We discuss two examples of microscopic CDW dynamics in some more detail: a size effect of phase-slip processes in $NbSe_3$ wires (Section 3) and negative resistances in (sub)micron segments of o-TaS_3 (Section 4).

2. Fabrication of mesoscopic CDW structures

We have developed three different techniques for the fabrication of submicron CDW devices. First, we combine an old technique — gluing thin CDW crystals on top of an

H S J van der Zant, N Marković, E Slot Department of Applied Sciences and DIMES, Delft University of Technology, Lorentzweg 1, 2628 CJ Delft, The Netherlands
N Marković Physics Department, Harvard University, 17 Oxford Street, Cambridge, MA 02138 USA

array of gold wires — with e-beam lithography to produce voltage probes that are spaced a few hundred nanometer apart. Second, patterning of $NbSe_3$ crystals has been performed to obtain 500 nm wide wires with voltage probes placed at distances as small as 500 nm as well. Third, the use of a focussed-ion beam (FIB) enables patterning of CDW crystals in almost any desired geometry. Figure 1 shows typical examples of all these three approaches which we will now discuss in more detail.

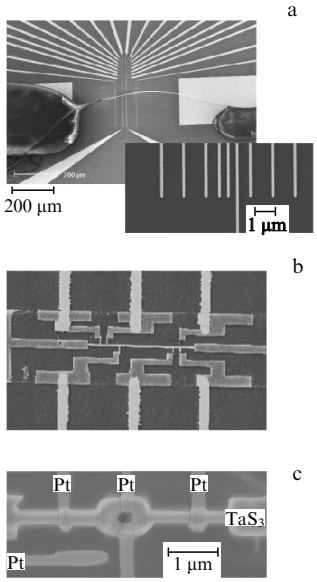

Figure 1. Several submicron CDW devices: a thin TaS_3 crystal glued on top of an array of voltage probes to study CDW dynamics on submicron length scales. The inset shows an enlargement of the main figure with 9 voltage probes that are 100 nm wide; the smallest distance between adjacent probes is 300 nm (a). A wire structure etched in a $NbSe_3$ crystal. The wire is 500 nm wide and 40 μm long. Several voltage probes are attached to the wire (b). A ring structure fabricated in a TaS_3 crystal using a focussed-ion beam. Platinum wires have been deposited in the same fabrication run (c).

To study microscopic CDW dynamics, the old technique of gluing crystals on metal leads can still be used provided that the probe width and spacing are made sufficiently small. In previous studies the smallest probe widths were of the order of 2 μm and their smallest separation of the order of 10 μm. By using standard e-beam lithographic techniques, we have fabricated an array of gold wires that are 50 nm high and 100 nm wide; the smallest probe separation is 300 nm (Fig. 1a). On o-TaS_3 crystals we have only obtained good electrical contact after heating them up to 120–130 °C for several minutes to one hour. During this annealing step, sulfur that has accumulated at the surface, oxidizes leaving behind a clean interface. For $NbSe_3$, we heat the samples so that the thin crystals do not start floating in the glue solvent. When the substrate is heated to 80 °C the solvent evaporates quickly, giving the crystal no opportunity to float.

The patterning of $NbSe_3$ crystals is discussed in detail in Ref. [3]. A 0.35 μm thin crystal, with typical dimensions of 4 mm along the crystallographic *b* axis and 27 μm along the *c* axis, is glued to a sapphire substrate. An aluminum etch mask is then defined on top by use of electron-beam lithography. Etching of the crystal occurs with a SF_6 plasma. In a second fabrication step, Au contacts are fabricated by near-UV optical lithography. A typical $NbSe_3$-wire structure is shown in Fig. 1b. The narrow part of the wire has a width of 0.5 μm and a length of 40 μm. Instead of directly contacting the wire by gold probes, we have patterned 0.5 μm wide voltage probes at the sides of the wire, within the $NbSe_3$ crystal. An advantage of this layout is the negligible shunting of current through the voltage probes. At the ends of the wire, 27×50 μm^2 large current pads are defined (not shown in Fig. 1b.

We found that the patterning process did not damage the crystals. The room-temperature resistivity of the wires is 0.2 mΩ cm, which is comparable to values for unpatterned crystals [4]. Measurements with various combinations of voltage contacts show that the resistivity is constant throughout the wire. Peierls transitions occur at $T_{P2} = 58$ K and $T_{P1} = 142$ K. The resistance ratio $R(295\text{K})/R(5\text{K})$ is 14 for a 0.5 μm wide wire, and 25 for a 1 μm wide wire. These ratios are lower than those for thick $NbSe_3$ crystals, but they compare well with values for thin unpatterned $NbSe_3$ crystals of comparable thickness [5]. Moreover, when biasing the sample with both a dc and ac signal, complete mode-locking is easily obtained with any probe pair.

The focussed-ion beam (FIB) promises to become an important tool for the definition of more complicated nano CDW-structures (see Fig. 1c). Crystals can be etched in almost any desired geometry with a resolution that is better than 100 nm. In addition, the FIB can deposit metal (e.g., Pt) structures with the same resolution so that contact can be made to the etched CDW devices without breaking vacuum. Obvious new directions are the study of finite size effects, the Aharonov–Bohm effect around single holes and the study of heterostructures combining CDWs with normal metal or superconductors. At present, we have only performed some first tests. Therefore in the remainder of this paper we will discuss results obtained from the other two fabrication methods.

3. Microscopic aspects of current conversion

Sliding CDWs can be visualized as moving wave fronts that are coupled by elastic forces. The motion of these wave fronts causes a compression of the CDW near one contact and a stretching near the other. Near contacts, phase slip events remove this strain [4, 5] by forming a local amplitude defect. The defect then grows across the whole cross-section, so that one complete wave front is added or removed. The rate at which wave fronts are added is determined by the strain amplitude. The CDW strain profile has been studied by several techniques, including electromodulated infrared transmission [6] and synchrotron X-rays [7, 8].

The displacement of the condensed electrons in the strained CDW causes an elastic force that is opposite to the applied field. In transport measurements, this opposite force must be overcome, leading to an additional voltage (V_{PS}) between the current contacts. Phase-slip has been extensively studied for bulk crystals [9–13]. Measurements on $NbSe_3$ crystals have shown that V_{PS} is length-independent for spacings larger than 20 μm [12]. We have studied the length dependence of V_{PS} down to micrometer length scales using the sample of Fig. 1b. We found a dramatic decrease of V_{PS} that is inconsistent with present theoretical models.

Figure 2a shows typical $I_{CDW}(V)$ characteristics in the normal and transposed four-terminal configuration. (In the

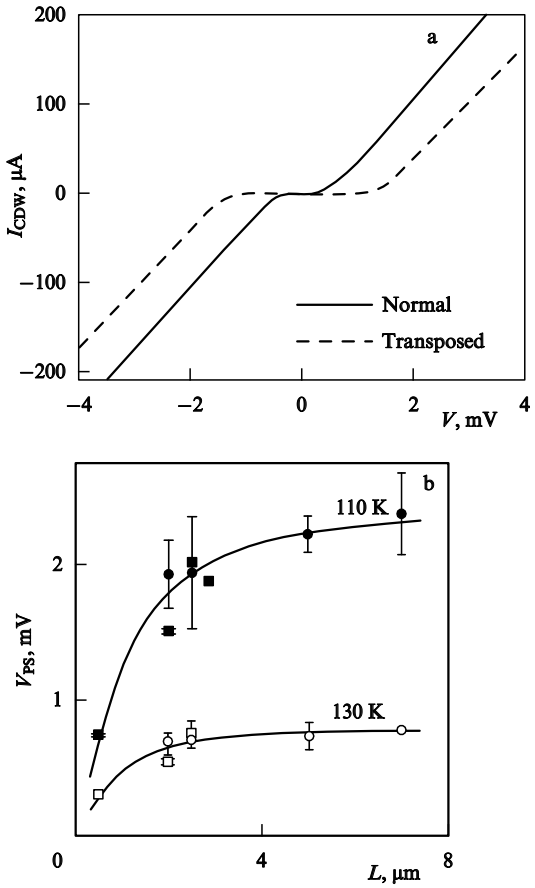

Figure 2. (a) CDW current versus voltage for 2 μm spaced contacts on a 1 μm wide wire (120 K). The solid line denotes a measurement in the normal configuration, whereas the dashed line represents data for the transposed configuration. V_{PS} is determined by subtracting the voltages for both curves at the same I_{CDW}. (b) Phase-slip voltage at $j_{CDW} = 57$ μA μm^{-2} versus contact spacing at two temperatures. Circles: 0.5 μm wide wire; squares: 1 μm wide wire. Curves are guides to the eye.

normal configuration, current is injected through the large probes connected at the ends of the wire while the voltage is measured with the small voltage probes; for the transposed configuration the current and voltage probes are exchanged.) An increase of I_{CDW} is observed beyond a well-defined threshold voltage. For the normal measurement, the onset of sliding-CDW transport occurs at $V_T = 0.24$ mV, corresponding to a threshold field $E_T = 1.2$ V cm^{-1}. For the transposed configuration, nonzero I_{CDW} is observed only for voltages larger than 1 mV. The difference between the curves is consistent with an additional phase-slip voltage required in the transposed configuration. By subtracting the measured voltages in transposed and normal measurements at, for example $I_{CDW} = 20$ μA, we find $V_{PS} = 0.9$ mV.

We have determined V_{PS} at several distances for both a 0.5 μm wire and a 1 μm wide wire. In Figure 2b the result is shown for two temperatures. The V_{PS} values for the 5 and 7 μm spacings are in good agreement with values found for unpatterned bulk crystals [14]. Between 3 μm and 0.5 μm, however, V_{PS} decreases by a factor of 2 to 3. Note that the data are taken at the same CDW current, i.e., the rate at which wave fronts are added (removed) is the same. Incomplete conversion cannot therefore be the reason for this dramatic decrease. To obtain the same I_{CDW}, incomplete conversion requires more strain so that a higher V_{PS} would then be measured. Existing models based on strain-induced nucleation of dislocation loops predict V_{PS} to increase as the contact spacing decreases. In the model by Ramakrishna et al. [15], strain falls off more rapidly when the contact spacing is reduced. For fixed V_{PS}, the region in which phase-slip processes occur is smaller and as a result, the CDW current decreases. More strain and, correspondingly, a higher V_{PS} is therefore required to produce the same CDW current.

We suggest that the reduction of V_{PS} is a mesoscopic effect [16] associated with the small dimensions of our sample. For bulk crystals, the number of wave fronts between the current contacts is large. Therefore, adding a single wave front will not significantly change the macroscopic strain profile. At micrometer length scales, however, the situation is different. For a $NbSe_3$ wire with a length of 1 μm, there are about 700 wave fronts between the current contacts. In the sliding state the CDW is compressed near one contact and stretched near the other with a typical change of the CDW wavelength of about 0.1% [7, 8]. This means that less than one additional wave front is accommodated in the compressed CDW and, similarly, less than one wave front is missing in the stretched CDW. If, in this situation, a single wave front is removed or added, the strain profile will be dramatically changed.

The reduction of V_{PS} for small contact spacings may be explained from such a collapse of the strain profile. After a phase-slip event, the strain at the contacts is strongly reduced or can even change sign. The sliding-CDW motion then restores the strain, until a new phase slip occurs. Therefore, there will be on average less strain in a mesoscopic wire. Since our measurements of V_{PS} are time-averaged values, a lower value of V_{PS} is expected. A quantitative description, however, has yet to be developed to describe current conversion at the micrometer scale and to explain the observed functional dependence of V_{PS} on L.

Another interesting phenomenon is present in the $I(V)$ curves measured on a small scale ($L < 5$ μm): they show step-like features resembling Shapiro steps as illustrated in Fig. 3. Note that we only observe these steps in the transposed configuration and that there is no ac drive applied. The step size is largely L- and T-independent, and corresponds to a frequency of the order of 100 MHz. A possible explanation may be the existence of self-induced Shapiro steps excited by standing phonon modes. A phonon velocity of 1000 – 3000 m s^{-1}, then yields a typical distance of the order of 20 – 60 μm. In Fig. 1b, the small wire is 40 μm long. More research (measurements on samples with different lengths) is needed and also theoretical modeling of this new effect would be helpful for a better understanding.

4. Local CDW dynamics in TaS_3

The characteristic length for CDW conductors lies in the micron range for phase correlation lengths and on the nanometer scale for the amplitude correlation length. Up to now, experiments have been concentrated on samples with dimensions well above 1 μm in the direction along metallic chains, and about 100 nm in the perpendicular directions. With probe spacings below the phase coherent lengths, one may expect new effects if pinning is no longer averaged over the sample volume. In this section, we report first measurements that reveal unexpected behavior on submicron scales including negative (differential) resistances in the current-voltage characteristics.

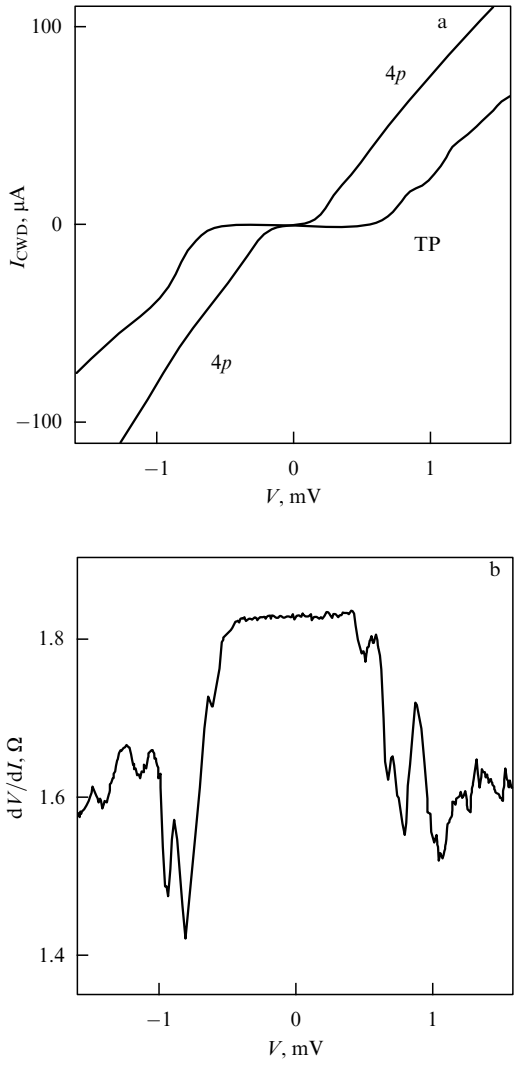

Figure 3. (a) CDW current versus voltage for 0.5 μm spaced contacts on a 1 μm wide wire (120 K). The inner curve denotes a measurement in the normal configuration showing no step-like features. The outer curve represents data for the transposed configuration and shows steps. (b) The differential resistance of the transposed measurement in (a) showing peaks at particular voltages resembling Shapiro steps.

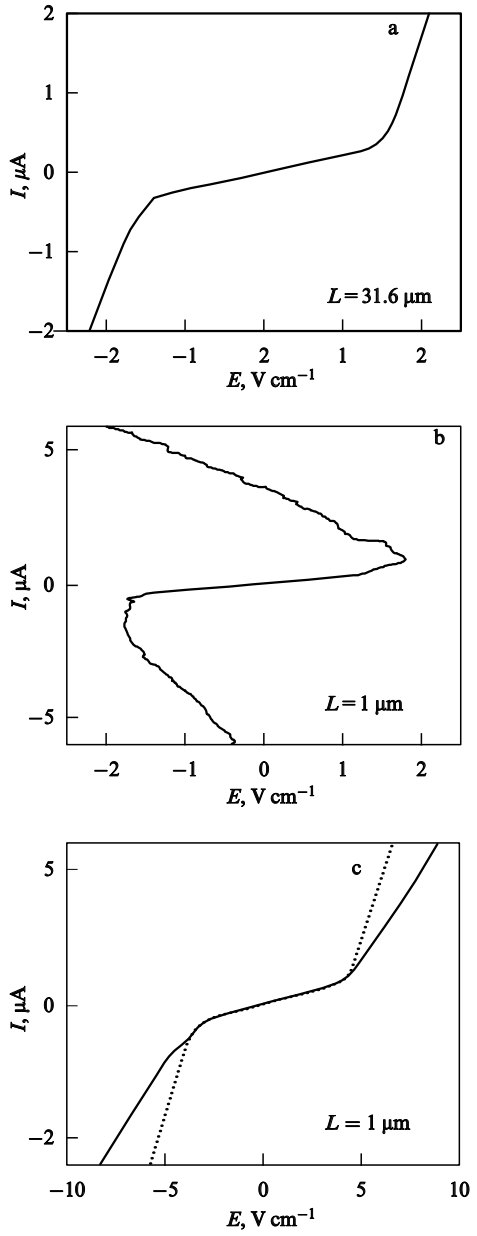

Figure 4. Three current – voltage characteristics of a TaS_3 crystal with a cross-section of 0.5 μm^2. The curves are taken on adjacent segments. In (a) the expected, averaged nonlinear CDW behavior is displayed. For high positive bias, the resistance becomes negative (b). The dashed lines (c) represent the $I(V)$ curve as expected from extrapolating the behavior on large length scales (see also text). Thus, the measured curve shows less CDW current at a given field, i.e., it is less nonlinear (c).

We have systematically studied the $I(V)$ characteristics of small segments of thin o-TaS_3 crystals placed on top of an array of small gold probes (see Fig. 1a). Figure 4 shows typical examples. The current is injected far away and various probe pairs measure the voltage between them (i.e., the normal configuration is used). When the probe spacing L is larger than about 10 μm, we always observe the expected behavior for CDWs as is illustrated in Fig. 4a.

On a micron scale, the shape of the $I(V)$ characteristic varies from segment to segment. Some small segments show the same nonlinear behavior as observed in the large segments. Other segments may yield an $I(V)$ that is less nonlinear (Fig. 4c) and sometimes we find $I(V)$ curves with a negative differential resistance (NDR). Occasionally the resistance may even become negative (see Fig. 4b), indicating that the moving CDW pumps charge carriers in the direction opposite to the applied field. But when measuring on larger length scales (even when including the segments that show different behavior), the deviations average out and differences between the various $I(V/L)$ curves are small. Thus, the characteristic length scale for the observation of N(D)R is of the order of a few micron. We have also studied the temperature dependence and find that N(D)R becomes visible at $T < 160$ K and more pronounced as the temperature is lowered. Note that we do not observe any unusual properties in the linear resistance R_0 nor the threshold field for the segments that show N(D)R. R_0 and V_T both scale with L within error margins for all probe distances.

An obvious candidate for the observation of NDR is the presence of heating effects. Because of the local character of the NDR and because the current probes are far away, we can

rule out this possibility. In early reports on CDW dynamics, NDR has also been observed in $NbSe_3$ crystals at low temperatures (45 K) accompanied by unusually large 1/f noise [17]. At even lower temperatures, these samples show switching events near threshold. The measurements [17] are performed with voltage probes spaced at macroscopic distances ($L \gg 100\,\mu m$). For $L > 5\,\mu m$, we have never seen NDR nor switching events in our TaS_3 crystals in the temperature range studied ($T > 90$ K).

We believe that the N(D)R we observe, originates from the response to local CDW deformations. Assuming that there are a few strong pinning centers or line dislocations in our crystal, strong deformations in the strain profile may be present around these regions. Strain leads to a shift of the chemical potential and this shift can be either up or down depending on the direction of sliding. For a semiconducting CDW with the Fermi level in the middle of the gap, a shift of the chemical potential leads to an increase of quasi-particles (either electrons or holes) and consequently to a decrease of the quasi-particle resistance. Such a resistance decrease may then produce regions with NDR as argued previously by Latyshev et al. [18] to explain NDR in their data on partly irradiated macroscopic samples. However, this reasoning cannot be used to explain a negative resistance: the decrease of the quasi-particle resistance cannot change the sign of the resistance. Most likely, nonequilibrium processes between the CDW and the quasi-particles must also play a role in this new phenomenon as well. No theory is available as yet.

Acknowledgements. The fabrication of the wire structure (Fig. 1b) has been performed in close collaboration with Yu I Latyshev, B Pannetier and P Monceau. The o-TaS_3 crystals were provided by R Thorne. The authors are grateful to Yu V Nazarov, Yu I Latyshev, S V Zaitsev-Zotov and S N Artemenko for useful discussions. This work is supported by the Netherlands Foundation for Fundamental Research on Matter (FOM). HSJvdZ is supported by the Dutch Royal Academy of Arts and Sciences (KNAW).

References

1. Grüner G *Density Waves in Solids* (Reading, Mass.: Addison-Wesley, 1994)
2. Peierls R, in *Quantum Theory of Solids* (Oxford: Oxford Univ. Press, 1955) p. 108
3. Mantel O C et al. *Synthetic Metals* **103** 2612 (1999)
4. Gor'kov L P *Pis'ma Zh. Eksp. Teor. Fiz.* **38** 76 (1983) [*JETP Lett.* **38** 87 (1983)]
5. Ong N P, Maki K *Phys. Rev. B* **32** 6582 (1985)
6. Itkis M E, Emerling B M, Brill J W *Phys. Rev. B* **52** R11545 (1995)
7. DiCarlo D et al. *Phys. Rev. Lett.* **70** 845 (1993)
8. Requardt H et al. *Phys. Rev. Lett.* **80** 5631 (1998)
9. Gill J C *Physica B* **143** 49 (1986)
10. Borodin D V, Zaitsev-Zotov S V, Nad' F Ya *Zh. Eksp. Teor. Fiz.* **93** 1394 (1987) [*Sov. Phys. JETP* **66** 793 (1987)]
11. Gill J C *Phys. Rev. Lett.* **70** 331 (1993)
12. Maher M P et al. *Phys. Rev. B* **52** 13850 (1995)
13. Lemay S G et al. *Phys. Rev. B* **57** 12781 (1998)
14. McCarten J et al. *Phys. Rev. B* **46** 4456 (1992)
15. Ramakrishna S et al. *Phys. Rev. Lett.* **68** 2066 (1992); Ramakrishna S *Phys. Rev. B* **48** 5025 (1993)
16. Mantel O C et al. *Phys. Rev. Lett.* **84** 538 (2000)
17. See, e.g., Hall R P, Sherwin M, Zettl A *Phys. Rev. Lett.* **52** 2293 (1984)
18. Latyshev Yu I, Pogotovsky N P, Artemenko S N *Synthetic Metals* **29** F415 (1989)

Mesoscopic physics on graphs

G Montambaux

Abstract. This report is a summary of recent work on the properties of phase coherent diffusive conductors, especially in the geometry of networks — also called graphs — made of quasi-1D diffusive wires. These properties are written as a function of the spectral determinant of the diffusion equation (the product of its eigenvalues). For a network with N nodes, this spectral determinant is related to the determinant of an $N \times N$ matrix which describes the connectivity of the network. I also consider the transmission through networks made of 1D ballistic wires and show how the transmission coefficient can be written in terms of an $N \times N$ matrix very similar to the above one. Finally I present a few considerations on the relation between the magnetism of noninteracting systems and the magnetism of interacting diffusive systems.

1. Return probability

Transport and thermodynamic properties of phase coherent disordered conductors can be described in a simple unified way: all can be related to the classical return probability $P(t)$ for a diffusive particle. I consider diffusive conductors, for which the mean free path l_e is much larger than the distance between electrons: $k_F l_e \gg 1$. The return probability has two components, a purely classical one (diffuson) and an interference term which results from interferences between pairs of time-reversed trajectories (Cooperon). The classical term is solution of the differential equation

$$[-i\omega - D\Delta]P_{cl}(\mathbf{r}, \mathbf{r}', \omega) = \delta(\mathbf{r} - \mathbf{r}')\,, \tag{1}$$

and the interference term is solution of the equation [1]:

$$\left[\gamma - i\omega - D\left(\nabla + \frac{2ie\mathbf{A}}{\hbar c}\right)^2\right] P_{int}(\mathbf{r}, \mathbf{r}', \omega) = \delta(\mathbf{r} - \mathbf{r}')\,, \tag{2}$$

whose solution has to be taken at $\mathbf{r}' = \mathbf{r}$. D is the diffusion coefficient. The scattering rate $\gamma = 1/\tau_\phi = D/L_\phi^2$ describes the breaking of phase coherence. L_ϕ is the phase coherence length and τ_ϕ is the phase coherence time. Finally, the space integrated (dimensionless) return probability is defined as

$$P(t) = \int P(\mathbf{r}, \mathbf{r}, t)\, d\mathbf{r}\,.$$

The *weak-localization* correction to the conductance can be written as [1]

$$\Delta\sigma = -s\frac{e^2 D}{\pi\hbar\Omega}\int_0^\infty P_{int}(t)\left[\exp(-\gamma t) - \exp\left(\frac{-t}{\tau_e}\right)\right] dt\,, \tag{3}$$

Ω is the volume and s is the spin degeneracy. The contribution of the return probability is integrated between τ_e, the smallest time for diffusion, and the phase coherence time $\tau_\phi = 1/\gamma$. Similarly, *the variance of the conductance fluctuations* at $T = 0$ K is given by

G Montambaux Laboratoire de Physique des Solides, associé au CNRS, Université Paris-Sud, 91405 Orsay Cedex, France